Eur. Phys. J. A **24**, 69–84 (2005)
DOI 10.1140/epja/i2004-10130-9

THE EUROPEAN
PHYSICAL JOURNAL A

Intranuclear-Cascade model calculation of photofission probabilities for actinide nuclei

I.A. Pshenichnov[1,2,a], B.L. Berman[1,b], W.J. Briscoe[1,c], C. Cetina[1,d], G. Feldman[1], P. Heimberg[1,e], A.S. Iljinov[2], and I.I. Strakovsky[1]

[1] Center for Nuclear Studies, Department of Physics, The George Washington University, Washington, D.C. 20052, USA
[2] Institute for Nuclear Research, Russian Academy of Science, 117312 Moscow, Russia

Received: 11 August 2004 / Revised version: 29 November 2004 /

Communicated by U.-G. Meißner

Abstract. We have calculated the fission probabilities for ^{237}Np, ^{233,235,238}U, ^{232}Th, and $^{\rm nat}$Pb following the absorption of photons with energies from 68 MeV to 3.77 GeV using the RELDIS Monte Carlo code. This code implements the cascade-evaporation-fission model of intermediate-energy photonuclear reactions. It includes multiparticle production in photoreactions on intranuclear nucleons, pre-equilibrium emission, and the statistical decay of excited residual nuclei via competition of evaporation, fission, and multifragmentation processes. The calculations show that in the GeV energy region the fission process is not solely responsible for the entire total photoabsorption cross-section, even for the actinides. The fission probabilities are 80–95% for ^{233}U, ^{235}U, and ^{237}Np, 70–80% for ^{238}U, and only 55–70% for ^{232}Th. This is because certain residual nuclei that are created by deep photospallation at GeV photon energies have relatively low fission probabilities. The results of those model calculations are in reasonable agreement (at the $\sim 10\%$ level) with recent experimental data on relative photofission cross-sections for ^{237}Np and ^{233,235,238}U (but not for ^{232}Th or $^{\rm nat}$Pb) from the Saskatchewan and Jefferson Laboratories over a very wide range in photon energy. Using our calculated fission probabilities plus the total photoabsorption cross-sections per nucleon, estimated from previous cross-section data for nuclei from C to Pb, we can infer absolute photofission cross-sections for the actinide nuclei and compare them with the SAL and JLab results. The resulting discrepancies, however, clearly demonstrate the need for direct measurement of the total photoabsorption cross-sections for the heavy actinides.

PACS. 25.20.-x Photonuclear reactions – 25.85.Jg Photofission – 24.10.Lx Monte Carlo simulations (including hadron and parton cascades and string breaking models)

1 Introduction

1.1 Relevant framework

Recently, high-precision experimental data have been obtained for the photofission of actinide and preactinide nuclei at the Saskatchewan Accelerator Laboratory (SAL) and Jefferson Laboratory (JLab) [1–4]. These data constitute both a challenge and an opportunity: a challenge to theory to reproduce them, and an opportunity to use them to determine the total photoabsorption cross-sections for these nuclei. Insofar as one can do this to sufficent accuracy, one can throw light on the concept of a "Universal Curve" for the photoabsorption cross-section per nucleon for all nuclei [5].

At this time, the only theory capable of reproducing these data is an extension of the widely known Intranuclear-Cascade (INC) model [6] to GeV photon-induced reactions [7], including subsequent evaporation and fission. Three decades ago, the INC model was successful in describing experimental data obtained with bremsstrahlung photons [8]. Later, the hybrid precompound-evaporation model approach of ref. [9] was successful in describing multiple photoneutron reactions below the pion production threshold.

A related subject is the electromagnetic dissociation of relativistic heavy ions, where virtual photons are used to initiate photonuclear reactions [10,11]. Recently, the INC

---

[a] *Present address*: Frankfurt Institute for Advanced Studies, J.-W. Goethe University, 60054 Frankfurt am Main, Germany.

[b] e-mail: `berman@gwu.edu`

[c] e-mail: `briscoe@gwu.edu`

[d] *Present address*: Naval Research Laboratory, Washington, D.C. 20375, USA.

[e] *Present address*: Bechtel-Nevada, Andrews Air Force Base, MD 20331, USA.

model [7] has been applied to the electromagnetic dissociation of ultrarelativistic heavy ions [12–15]. In such reactions, nuclei are disintegrated by virtual photons over the wide energy range from a few MeV to a few tens of GeV. A Monte Carlo code called RELDIS (Relativistic ELectromagnetic DISsociation) was devised to perform calculations for real and virtual photons across this wide energy range.

We now use the RELDIS code to describe the recent photofission data [1–4]. This paper reports our results and their potential implications. The description of the RELDIS model of photonuclear reactions is given in sect. 2. Calculational results for nuclear-fission probabilities and absolute photofission cross-sections (assuming the "Universal Curve" for the photoabsorption cross-section per bound nucleon) are presented in sect. 3. We summarize our findings in sect. 4.

1.2 Experimental background

As first pointed out by Bohr and Wheeler [16] and echoed by Aage Bohr [17], the relative simplicity and directness of the electromagnetic interaction is very useful in the exploration of the process of nuclear fission. At the first stage of a photonuclear reaction, the absorption of a photon on a pair of intranuclear nucleons brings in only thermal energy and produces fewer changes in the structure of the target nucleus than, for example, reactions induced by protons or antiprotons. In the latter cases, the antiproton annihilation removes an intranuclear nucleon, or, respectively, the projectile nucleon can be trapped by the nuclear potential. Therefore, one can expect that following photoabsorption at low energies, most of the fissioning nuclides are similar to the target nucleus. This makes photofission studies much more transparent.

Over the years, photon-induced fission has attracted attention, and considerable progress has been made in experimental photofission studies. In the Giant Dipole Resonance (GDR) region, experiments at Livermore [18–20] and elsewhere delineated the giant-resonance parameters with high accuracy for eight actinide isotopes (^{232}Th, ^{237}Np, ^{239}Pu, and the five long-lived uranium isotopes). At these low energies (from threshold to about 20 MeV), photofission reveals its simplicity, and the total photoabsorption cross-section equals the sum of the single- and double-photoneutron cross-sections plus the photofission cross-section, since the high Coulomb barrier greatly inhibits the emission of charged particles.

In the quasideuteron and $\Delta(1232)$ regions, experiments at Saclay [21], Mainz [22], and elsewhere extended the photofission data to intermediate energies for ^{235,238}U and ^{232}Th. From a comparison of the photofission cross-sections per nucleon for these nuclei with the total photoabsorption cross-sections per nucleon obtained by other methods at Mainz [23], Frascati [24], and Bonn [25], it was commonly believed that there was a "Universal Curve" and that the photofission cross-section for ^{238}U saturates the total cross-section. Contrary to this opinion, the ratio of ^{237}Np to ^{238}U photofission cross-sections in the energy range 60–240 MeV measured at Novosibirsk was reported to be about 1.2–1.4 [26,27], with the implication that only the fissility for ^{237}Np might approach unity. The latter finding confirms earlier results [28] for the ratio of ^{237}Np to ^{238}U photofission cross-sections in the energy range 150–710 MeV. The inelastic Bethe-Heitler process of e^+e^--pair production accompanied by fission was considered in refs. [28,27] as an additional photon-induced fission channel, but its contribution was found to be insufficient to explain the excess of the ^{237}Np photofission cross-section over the "Universal Curve."

The recent precise data from SAL [1,2] agree well with the earlier data across the upper part of the quasideuteron region (about 60 MeV to the photopion threshold) and the lower part of the $\Delta(1232)$ region (up to about 250 MeV). The recent data from JLab [3,4] extend our knowledge of the photofission cross-sections for ^{237}Np, ^{233,235,238}U, ^{232}Th, and $^{\mathrm{nat}}$Pb across the $\Delta(1232)$ region and through the higher-resonance region (from 0.20 to 3.77 GeV). In particular, this gives us the opportunity to investigate the relationship between the ^{237}Np and ^{238}U photofission cross-sections and the "Universal Curve" over a much wider photon energy range than was possible heretofore [26,27]. In this energy domain, photonuclear reactions seem to be more complicated. New advanced theoretical models must be employed to account for the greater number of reaction channels that are open during the first step of the reaction due to meson photoproduction on the intranuclear nucleons. Also, the understanding of the role of nuclear fission among the many other decay modes of the excited nucleus requires a well-founded theoretical model to describe such decay.

1.3 Theoretical approaches to describe photofission

One of the first calculations using the Intranuclear-Cascade (INC) model that includes photon absorption at intermediate energies was that of ref. [8]. This calculation takes into account the channels of the γN interaction with production of only one or two pions, and thus can be applied at photon energies only up to 1 GeV. It was tested with old experimental data obtained with bremsstrahlung photons. Later, the model was successfully applied to early photofission studies [29–31].

INC model predictions [8,30] for the first pre-equilibrium stage of the photofission reaction were also used in fission probability calculations for ^{232}Th and ^{238}U nuclei by introducing the mean-compound-nucleus approximation [32]. According to this method, the ensemble of excited residual nuclei created after the first step of a photonuclear reaction is replaced by a single excited nucleus with the average values of neutrons N, protons Z, and excitation energy $E^\star$. In order to explain the data on thorium, one needs to account for its higher nuclear transparency relative to uranium [32]. Such a difference for nuclear systems of comparable mass was attributed to subtle details of the nuclear structure of ^{232}Th and ^{238}U. The nature and origin of such differences still need to be explained. The fissility of ^{238}U was assumed to be saturated; that is, its fission probability $W_{\mathrm{f}} \equiv \sigma_{\mathrm{f}}/\sigma_{\mathrm{tot}}$ was assumed to be unity.

Another phenomenological method was proposed in ref. [33] to describe the photofission of ^{209}Bi, ^{232}Th, and ^{238}U in the quasideuteron region, $E_\gamma = 30$–140 MeV. A special phenomenological factor, which is related to the probability of the quasideuteron absorption that leads to photofission, was introduced and was found to be different for ^{209}Bi than for ^{238}U.

In refs. [34,35], the photofissility of actinide nuclei at intermediate energies was considered within the multicollisional model for photon-induced intranuclear-cascade process and the statistical neutron evaporation and fission models for de-excitation of residual nuclei. The fission probabilities for both ^{237}Np and ^{238}U were found to be unsaturated, *i.e.* very close, but still less than unity. However, the authors of refs. [34,35] considered their approach to be accurate only in a restricted range of photon energies, from 0.5 GeV to 1 GeV. This makes difficult a direct comparison with the SAL and JLab data [1–4], since the data were obtained over a much wider energy range, from 68 MeV to 3.77 GeV.

Recently, the range of applicability of the INC model was extended up to 10 GeV [7]. The accuracy of the model was improved from the photoneutron thresholds up to 2 GeV, and new data obtained with monochromatic photons were used to verify the model predictions. The analysis of photofission reactions performed in the present paper is based on this approach, which is free of the simplifications and assumptions made in refs. [32,33] and is valid for a much wider region of incoming photon energies than the approach of refs. [34,35].

The following questions are addressed here:

1) Is it possible to describe the photofission of actinide nuclei over such a broad energy range, and if so, how good is this description?
2) Does the relative simplicity of low-energy photonuclear reactions persist at photon energies above 1 GeV, where multiple photoproduction of hadrons takes place?
3) To what extent does the excited residual nucleus, created after the first stage of the photonuclear reaction, retain the properties of the target nucleus?
4) Can the absolute photofission cross-sections for heavy actinide nuclei be obtained from the calculated fission probabilities and the total photoabsorption cross-sections per nucleon for $A \leq 208$ nuclei?
5) Can the total photoabsorption cross-sections be obtained from the calculated fission probabilities and the measured photofission cross-sections? What is the level of calculational and experimental uncertainties in the determination of the total photoabsorption cross-section for heavy actinides in this way?

In order to answer these questions, we use the model with its main parameters extracted from independent studies [7,12,13,29,30,36–38] of photon–, hadron–, and heavy-ion–induced reactions, in contrast to other approaches [32–35], where only photon-induced reactions were considered. The present theoretical investigation is aimed at estimating the characteristics of the first step in the photoabsorption process and determining the total fission probability for such a reaction.

2 The RELDIS model of photonuclear reactions

2.1 Initial interaction and intranuclear cascade of photoproduced hadrons

The fast hadrons produced in a primary γN or NN interaction initiate a cascade of successive hadron-nucleon collisions inside the target nucleus during the first, nonequilibrium, stage of the photonuclear reaction. The duration of this stage τ_{cas} can be estimated as the time a fast particle needs to cross the nucleus: $\tau_{\mathrm{cas}} \sim \tau_0$, where $\tau_0 \leq 10^{-22}$ s.

The INC model is a numerical method to solve the kinetic equation that describes hadron transport in the nuclear medium. Calculations of intranuclear cascades were performed by using a Monte Carlo technique. The nucleus is considered to be a mixture of degenerate Fermi gases of neutrons and protons in a spherical potential well with a diffuse boundary. By using the effective real potentials of nucleons and pions, the influence of intranuclear nucleons on these cascade particles is taken into account. The momentum distribution of intranuclear nucleons is calculated in the local-density approximation of the Fermi-gas model. The distribution of nuclear density is approximated by a set of step-like functions. The cross-sections of elementary collisions $NN \to NN$, $NN \to \pi NN$, $\pi N \to \pi N$, $\pi N \to \pi\pi N$, $\pi NN \to NN$, … in the nuclear medium are assumed to be the same as in vacuum except that using the Pauli principle prohibits transition of the cascade nucleons into the states already occupied by the intranuclear nucleons. A more detailed description of the INC model is given in ref. [6].

By means of the INC model, the process of dissipation of the initial photon energy can be investigated in detail. Part of this energy is transformed into internal excitation of the residual nucleus; the rest is released by fast cascade hadrons leaving the nucleus.

2.2 Creation of an excited compound nucleus

At the end of the hadronic cascade, some quasiparticles remain in the nuclear Fermi gas as "holes" (N_{h}), which are knocked-out nucleons, and particles (N_{p}), which are slow cascade nucleons trapped by the nuclear potential. In the INC model, the excitation energy of the residual nucleus is defined as

$$E^\star = \sum_{i=1}^{N_{\mathrm{p}}} \epsilon_i^{\mathrm{p}} + \sum_{i=1}^{N_{\mathrm{h}}} \epsilon_i^{\mathrm{h}}, \qquad (1)$$

where the quasiparticle energies for particles ϵ_i^{p} and holes ϵ_i^{h} are measured with respect to the Fermi energy. The numbers of nucleons and protons of the residual nucleus are given by the relations

$$A_{\mathrm{RN}} = A - \sum_{i=1}^{N_{\mathrm{c}}} q_i^{\mathrm{c}} \tag{2}$$

and

$$Z_{\mathrm{RN}} = Z - \sum_{i=1}^{N_{\mathrm{c}}} e_i^{\mathrm{c}}, \tag{3}$$

where A and Z are the numbers of nucleons and protons, respectively, in the target nucleus, and q_i^{c} and e_i^{c} are the baryon number and charge carried away by the cascade particle i.

The moment when all fast particles have left the nucleus marks the beginning of the period of the establishment of thermal equilibrium in the residual nucleus with a duration of $\tau_{\mathrm{peq}} \sim (10\text{–}100) \cdot \tau_0$. At the end of this period, thermal equilibrium is reached and an excited compound nucleus has been created.

Various criteria may be applied to decide whether the nuclear system has reached thermal equilibrium. According to the exciton model [39], the system of Fermi particles created after the cascade stage is not in equilibrium if the number of quasiparticles $N_{\mathrm{q}} = N_{\mathrm{p}} + N_{\mathrm{h}}$ is less than the equilibrium value $N_{\mathrm{q}}^{\mathrm{eq}} \sim \sqrt{2gE^\star}$, where g is the density of single-particle states. Therefore, in the course of the equilibration process, pre-equilibrium particles may be emitted. In our calculations, the pre-equilibrium exciton model [39] is used to simulate pre-equilibrium emission.

Relative probabilities of the de-excitation processes are determined by the excitation energy $E^\star$ and by the mass A_{RN} and charge Z_{RN} of the residual nucleus formed after the establishment of thermal equilibrium.

Depending on the photon energy E_γ, various processes may contribute to the energy deposition. In the following, we consider step by step all of these mechanisms, with special attention to the amount of energy that is transformed into internal excitation of the nucleus.

Figure 1 shows the average excitation energy $E^\star$ and the fraction of E_γ that on average is transformed into $E^\star$ in photoabsorption on $^{\mathrm{nat}}$Pb, ^{232}Th, and ^{237}Np. The average values of $E^\star$ per nucleon of the residual nucleus $\langle E^\star / A_{\mathrm{RN}} \rangle$ also are shown in fig. 1.

As shown by calculations, when a nucleus absorbs a photon in the GDR region ($6 \leq E_\gamma \leq 30$ MeV), its energy is almost completely transformed into excitation energy $E^\star$. For a preactinide nucleus like Pb, whose fission threshold is above 20 MeV, the de-excitation proceeds mainly through the evaporation of neutrons, since their separation energies are only about 7 MeV. Due to the high Coulomb barrier in heavy nuclei, proton emission is suppressed in the GDR region. Fission thresholds are much lower for the actinides; *e.g.*, for U and Np, it is ≤ 6 MeV [18], and the fission channel dominates in the decay of such nuclei even at low excitation energies [18–20].

Starting from $E_\gamma = 30$ MeV, where the quasideuteron mechanism becomes important, up to the single-pion production thresholds at $E_\gamma \simeq 140$ MeV, only a small part of the photon energy is converted (on average) into the excitation energy $E^\star$ of the residual nucleus. The rest of the photon energy is taken away by the fast nucleons originating from the absorbing pair. It was deduced from experimental data [40] that $E^\star = 43.4 \pm 5$ MeV for photoabsorption on lead at $E_\gamma = 70$ MeV. The prediction of our model agrees well with this value, as seen in fig. 1a.

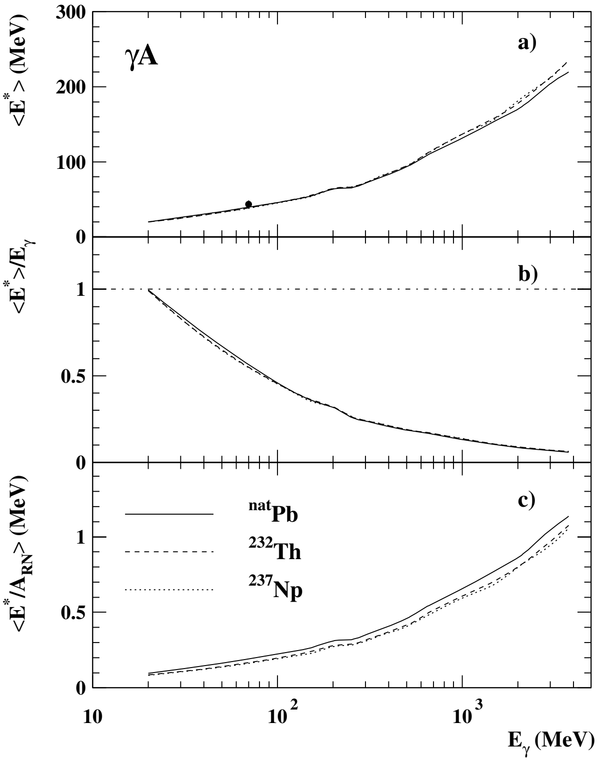

Fig. 1. a) Average excitation energy of the residual nucleus $\langle E^\star \rangle$ following photoabsorption. b) Ratio of the average excitation energy of the residual nucleus $\langle E^\star \rangle$ to the input photon energy E_γ. c) Average values of $E^\star$ per nucleon of the residual nucleus. The RELDIS code results are given by solid, dashed, and dotted lines for $^{\mathrm{nat}}$Pb, ^{232}Th, and ^{237}Np, respectively. The value for $\langle E^\star \rangle$ deduced from an experiment on the photoabsorption for lead [40] is denoted by the data point.

The two-nucleon absorption cross-section of a photon on a heavy nucleus $\sigma_{\gamma A}^{\mathrm{QD}}$ is taken from the quasideuteron model of Levinger [41], as modified in ref. [42]:

$$\sigma_{\gamma A}^{\mathrm{QD}} = kZ(1 - Z/A)\sigma_d^{\mathrm{exch}}. \tag{4}$$

Here σ_d^{exch} is the meson exchange part of the cross-section σ_d for deuteron photodisintegration, $\gamma d \to np$ [43], A and Z are the mass and charge numbers of the relevant nucleus, and $k \approx 11$ is an empirical constant taken from the analysis of ref. [42].

Although the cross-section σ_d decreases strongly with photon energy, the two-nucleon absorption mechanism competes with the single-nucleon photoabsorption channel $\gamma N \to \pi N$ even up to $E_\gamma \sim 500$ MeV, when the wavelength of the incident photon becomes much smaller than the internucleon spacing.

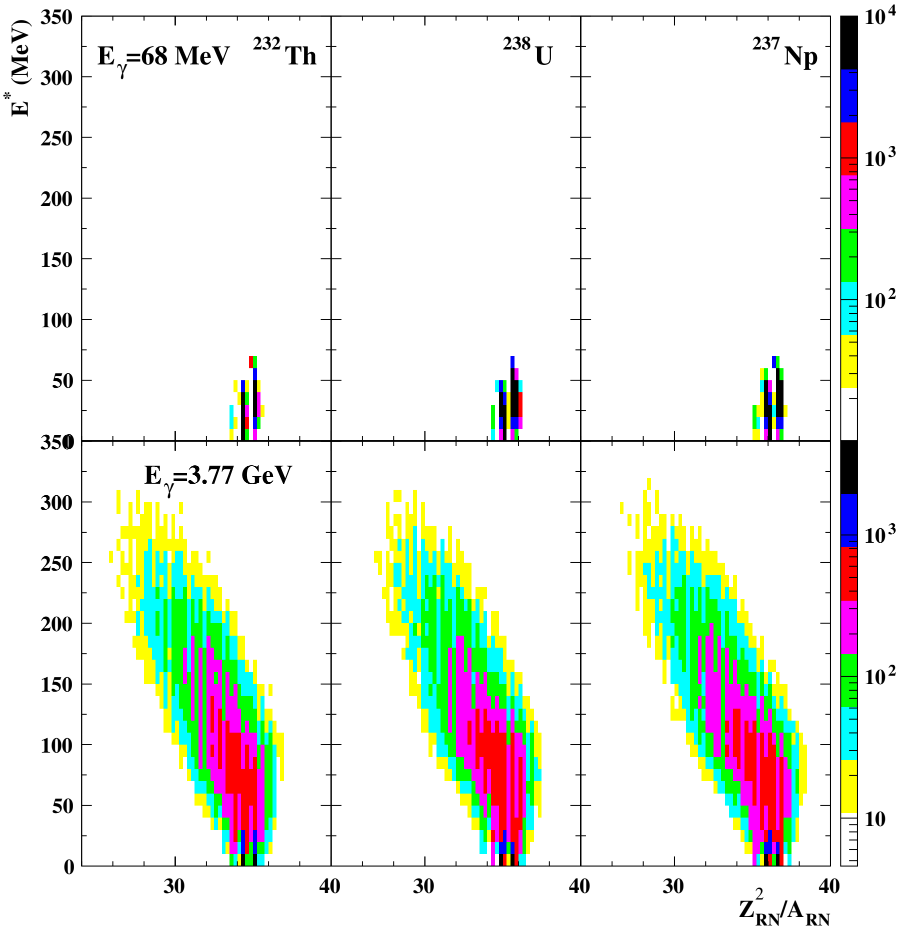

Fig. 2. Distributions of $E^{\star}$ and $Z^2_{\mathrm{RN}}/A_{\mathrm{RN}}$ for residual nuclei created after the fast stage of the photoabsorption process for $E_\gamma = 68$ MeV (top) and for $E_\gamma = 3.77$ GeV (bottom), for ^{232}Th, ^{238}U, and ^{237}Np (left to right). The same number (10^5) of residual nuclei is shown for each case.

An interesting effect concerning the photon energy dissipation above the $\gamma N \to \pi N$ threshold was noticed in ref. [31]. A pion of 50–100 MeV has a small interaction cross-section with nucleons and therefore has a high probability to carry away a large part ($\approx m_\pi$) of the photon energy. Only at $E_\gamma \approx 250$ MeV does the average value $\langle E^{\star}\rangle$ start to increase, as shown in fig. 1.

The reliability of the model predictions for $E^{\star}$ can be tested by the comparison of the calculated first and second moments of multiplicity distributions of neutrons, $\langle N_n\rangle$ and $W_n = \sqrt{\langle N_n^2\rangle - \langle N_n\rangle^2}$, with the experimental data of ref. [40]. In photoabsorption on lead, most of the neutrons are emitted via evaporation from excited compound nuclei, and both $\langle N_n\rangle$ and W_n are sensitive to $E^{\star}$. This test was performed in ref. [13] and $\langle N_n\rangle$ and W_n were found to be described with an accuracy of 10–15% at $70 \le E_\gamma \le 140$ MeV.

Above the two-pion production threshold, at $E_\gamma \sim 400$ MeV, the photon-nucleon (γN) interaction becomes more complicated because of the opening of many possible final states. We use a phenomenological model for the description of the γN interaction, developed in ref. [7]. The model includes not only the excitation of nucleon resonances, but also both the resonance contribution from the two-body channels, $\gamma N \to \pi B^{\star}$ and $\gamma N \to M^{\star} N$ ($B^{\star}$ and $M^{\star}$ being baryon and meson resonances) and the non-resonant contribution from the multiple-pion production channels $\gamma N \to i\pi N$ ($2 \le i \le 8$). Finally, when the photon energy reaches a value of a few GeV, multiple-pion production becomes the dominant process. A large number (~ 80) of many-body subchannels are included in our calculation.

Since the cross-section $\gamma N \to$ hadrons is small compared to the total NN or πN cross-sections, this leads to a large number of photons leaving the nucleus without producing hadrons in the case of direct use of a Monte Carlo simulation technique. This is a natural consequence of the well-known fact that nuclei are highly transparent to photons (*i.e.*, photons do not interact strongly). In order to reduce the computation time, we simulate photon absorption in each event, but in this case we have to normalize our simulated results to the total photonuclear cross-section to get the absolute fission cross-sections.

At high photon energies, many hadrons are produced inside the target nucleus in the course of a cascade process. Due to the knockout of intranuclear nucleons by fast nucleons and pions, the slower particles pass through a lower-density region, thereby undergoing fewer rescatterings; this is the so-called "trawling" effect. As was shown in refs. [37,36,44], the trawling effect is important for a realistic description of reactions at projectile energies above several GeV. In the present calculation, we use a nonlinear version of the INC model [36], which takes into account the local depletion of nuclear density during the development of the intranuclear cascade.

In summary, as can be seen from fig. 1, when the photon energy increases from the GDR region to several GeV, the nature of the photoabsorption process evolves from the excitation of collective nuclear degrees of freedom to the excitation of a single nucleon inside the nucleus. In the latter case, up to 95% of the photon energy is released in the form of fast particles leaving the nucleus. Nevertheless, the remaining energy deposited in the compound nucleus is sufficient for evaporating many neutrons and thus leading to fission, since neutron evaporation increases the fissility parameter Z^2/A. However, fig. 1 shows only the average values; the entire distribution of excitation energy $E^\star$ is shown in fig. 2. In high-energy photoabsorption the $E^\star$ distribution is very wide, since some of the reaction channels lead to strong heating of the nucleus by a multipion system.

As shown in fig. 1, the excitation energies of residual nuclei produced in photoabsorption on lead, thorium, and neptunium are very close to each other, despite some differences in the masses of the target nuclei. Therefore, one can expect that the dramatic differences in fission probabilities in photoabsorption on such target nuclei are due to differences in fissility parameters for these ensembles of residual nuclei, rather than in their excitation energies. Figure 2 confirms this expectation. In fig. 2, the values of $E^\star$ and the liquid-drop–model fissility parameter $Z^2_{\mathrm{RN}}/A_{\mathrm{RN}}$ are given for the whole ensemble of excited residual nuclei created after the cascade stage of photoabsorption at E_γ values of 68 MeV and 3.77 GeV for ^{232}Th, ^{238}U, and ^{237}Np.

As one can see in fig. 2, at $E_\gamma = 3.77$ GeV, residual nuclei are created with very broad distributions in excitation energy, $0 < E^\star < 300$ MeV, and fissility parameter, $26 < Z^2_{\mathrm{RN}}/A_{\mathrm{RN}} < 38$. At higher photon energies, these broad distributions are determined mainly by the variations of the number of pions and nucleons participating in the cascade flow. Such variations are due to the wide variety of open channels in the primary γN interaction and in the secondary πN and NN interactions with intranuclear nucleons. Taken alone, the variation in the number of cascade nucleons due to different impact parameters in a photonuclear interaction cannot provide such broad distributions. Indeed, the impact parameter distributions of photonuclear interaction events are similar for $E_\gamma = 68$ MeV and 3.77 GeV; but in the former case, the distributions in $Z^2_{\mathrm{RN}}/A_{\mathrm{RN}}$ are quite narrow. This is explained by the fact that only a limited number of channels are open at $E_\gamma = 68$ MeV, namely $\gamma + (pn) \rightarrow p + n$ and channels of the NN interaction below the pion photoproduction thresholds.

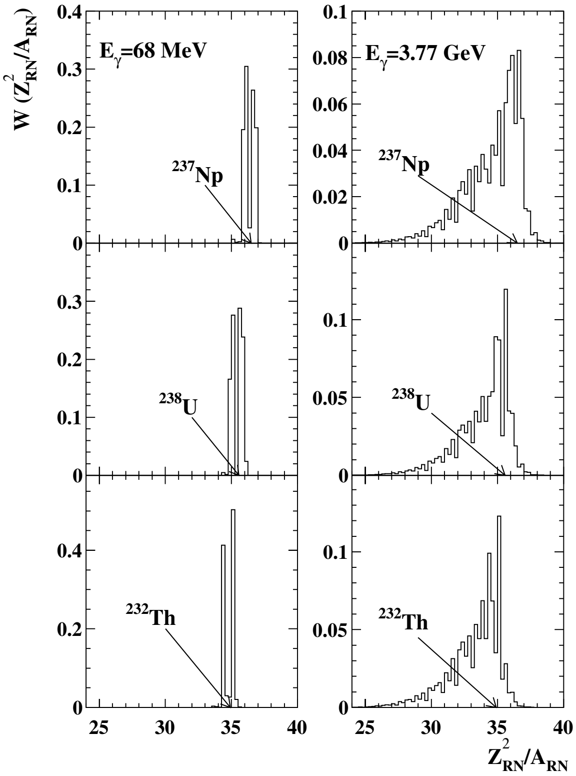

Fig. 3. Probability distributions of $Z^2_{\mathrm{RN}}/A_{\mathrm{RN}}$ for residual nuclei created after the fast stage of the photoabsorption process, for $E_\gamma = 68$ MeV (left) and for $E_\gamma = 3.77$ GeV (right), for ^{237}Np, ^{238}U, and ^{232}Th, top to bottom. The values of Z^2/A for the target nuclei are shown by the arrows.

At higher photon energy, $E_\gamma \geq 1$ GeV, the photoabsorption process reveals its complexity and the mean-compound-nucleus approximation used in ref. [32] for fission probability calculations breaks down. This is demonstrated in fig. 3, where the fissility parameter distributions of the residual nuclei are shown for $E_\gamma = 68$ MeV and 3.77 GeV. Strictly speaking, the approximation used in ref. [32] is not valid even at $E_\gamma = 68$ MeV, since basically two types of photonuclear reactions occur: preferential removal of protons, which decreases $Z^2_{\mathrm{RN}}/A_{\mathrm{RN}}$, and preferential removal of neutrons, which increases of $Z^2_{\mathrm{RN}}/A_{\mathrm{RN}}$. Therefore, the ensemble of residual nuclei created at low energies, particularly below the pion production thresholds, can be represented by a pair of "characteristic" compound nuclei. The first group of nuclei, whose values of $Z^2_{\mathrm{RN}}/A_{\mathrm{RN}}$ are less than that for the target nucleus, is created mainly via (γ, p), (γ, pn), and $(\gamma, p2n)$ reactions, while the second group is created via (γ, n), $(\gamma, 2n)$, and $(\gamma, 3n)$ reactions. However, as shown in fig. 3, this approximation for the ensemble of residual nuclei becomes invalid in the GeV region, where a very wide set of residual nuclei is created following the fast stage of photoabsorption. An example of such a distribution is shown in fig. 4 for photoabsorption in ^{237}Np. In the course of the cascade process, the target nucleus loses up to ~ 30 units in charge and up to

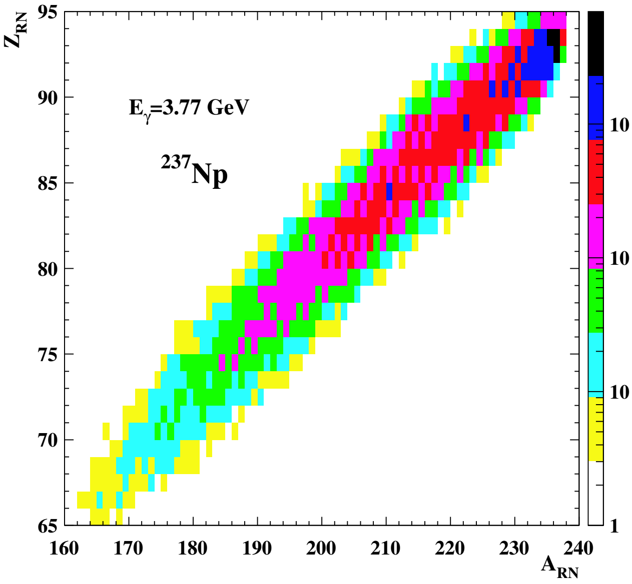

Fig. 4. Distribution of masses and charges of excited residual nuclei created after the fast stage of the photoabsorption process for $E_\gamma = 3.77$ GeV in ^{237}Np.

$\sim$ 70 nucleons. Highly excited preactinide nuclei, like Pb or Au, can be created in photoabsorption reactions at high photon energies. Poorly explored nuclei with A and Z located between Po and Th are also represented in fig. 4. In our calculations, we take into account the whole ensemble of excited compound nuclei without replacing it by a "characteristic" average compound nucleus.

2.3 Decay of the excited compound nucleus

As soon as statistical equilibrium is reached in the residual nucleus, the statistical approach for nucleon and light-particle evaporation and nuclear fission is an appropriate scheme for the calculation of the relative probabilities of different decay modes of the compound nucleus. Such statistical decay of the compound nucleus is the slow stage of the photonuclear reaction, having a characteristic time $\tau_{\mathrm{evf}} \gg \tau_0$. Here we use the term "residual nucleus" to mean the nuclear residue formed at the end of the intranuclear cascade, while the term "compound nucleus" is used to describe a residual nucleus after the establishment of thermal equilibrium.

In the domain of modest excitation energies, which are typical for heavy nuclei, with $E^\star/A_{\mathrm{CN}} \leq$ 2–3 MeV, one can include the competition between evaporation and fission only; the onset of multifragmentation is located well above this range at $E^\star/A_{\mathrm{CN}} > 4$ MeV [38]. As can be seen in fig. 2, there are no residual nuclei with $E^\star/A_{\mathrm{RN}}$ exceeding ~ 1.3 MeV, even at $E_\gamma = 3.77$ GeV. Therefore, we do not expect any contribution of the multifragmentation process to photoabsorption on heavy nuclei.

According to the standard Weisskopf evaporation scheme [45], the partial width Γ_j for the evaporation of a particle $j = n, p, {}^2\mathrm{H}, {}^3\mathrm{H}, {}^3\mathrm{He}$, or ^{4}He is given by

$$\Gamma_j = \frac{(2s_j+1)\mu_j}{\pi^2 \rho_{\mathrm{CN}}(E^\star)} \int\limits_{V_j}^{E^\star - B_j} \sigma^j_{\mathrm{inv}}(E)\rho_j(E^\star - B_j - E)E\mathrm{d}E \ , \tag{5}$$

where s_j, μ_j, V_j, and B_j are the spin, reduced mass, Coulomb barrier, and binding energy of the particle j, respectively. $\sigma^j_{\mathrm{inv}}(E)$ is the cross-section for the inverse reaction of the capture of the particle i to create the compound nucleus. ρ_{CN} and ρ_j are the nuclear level densities for the initial and final (after the emission of the particle j) nuclei, respectively. Natural units, with $\hbar = c = 1$, are used in this paper.

The Bohr-Wheeler statistical approach [16] is used to calculate the fission width of the excited compound nucleus. This width is proportional to the nuclear level density ρ_{f} at the fission saddle point:

$$\Gamma_{\mathrm{f}} = \frac{1}{2\pi \rho_{\mathrm{CN}}(E^\star)} \int\limits_{0}^{E^\star - B_{\mathrm{f}}} \rho_{\mathrm{f}}(E^\star - B_{\mathrm{f}} - E)\mathrm{d}E \ , \tag{6}$$

where B_{f} is the fission barrier height. Masses and kinetic energies of fission products are calculated based on corresponding approximations [46] to experimental data which describe the transition from the asymmetric fission mode to the symmetric one, along with other features of the fission process. Since the masses of fission fragments were not measured in the experiments reported in refs. [1–4], we do not consider such distributions in this work.

The decay of the excited compound nucleus is simulated using the Monte Carlo method. The competition between the various decay channels at each step of the evaporation chain is determined by the relation between the partial widths for particle evaporation and fission, eqs. (5) and (6), respectively. Finally, in order to calculate the fission probability W_{f}, the total number of fission events in a computer run is counted and divided by the total number of simulated photoabsorption events. Evaporation from excited fission fragments is also taken into account and was found to be negligible.

In the present paper, we also take into account the microscopic effects of nuclear structure in the nuclear-mass and level-density formulas, according to refs. [47–49]. Such effects reveal themselves as a noticeable difference, up to $\sim$ 10–15 MeV for heavy closed-shell nuclei, between the values of the measured nuclear ground-state masses $M_{\mathrm{exp}}(Z,N)$ and those predicted by the macroscopic liquid-drop model $M_{\mathrm{LD}}(Z,N)$ [50]. Moreover, this difference in mass $\delta W_{\mathrm{gs}} = M_{\mathrm{exp}}(Z,N) - M_{\mathrm{LD}}(Z,N)$, the so-called shell correction, and the level-density parameter a (used in eq. (7) below) are strongly correlated. For closed-shell nuclei, the actual values of the level-density parameter are substantially lower than the average values of $A/8$–$A/10$ MeV^{-1}, and these values depend strongly on the excitation energy. Proper accounting for these effects, as well as for pairing effects, is important mainly at low excitations, for $E^\star \sim 10$ MeV. Although these shell effects are very pronounced at low excitation energies, they disappear for $E^\star \geq 30$ MeV [49,51]. Several phenomenological approximations of the level-density parameter were proposed in order to account for such behavior. Our calculations are based mainly on the results of ref. [49], where the data on the level densities, decay widths, and lifetimes of excited nuclei with $2 < E^\star < 20$ MeV have been analyzed in the framework of the statistical model.

We use the Fermi-gas expression for the nuclear level density at excitation energy $E^\star$:

$$\rho(E^\star) = \frac{\sqrt{\pi}}{12 E^{\star 5/4} a^{1/4}} \cdot \exp\{2\sqrt{aE^\star}\}\ , \tag{7}$$

where $a = \pi^2 g_\mathrm{F}/6$ is the nuclear level-density parameter, which is proportional to the density of single-particle states g_F at the Fermi surface.

Pairing-energy effects are accounted for by the substitution $E^\star \to E^\star - \Delta$, where the pairing energy Δ is given by

$$\Delta = \chi \cdot 11/\sqrt{A}\ \mathrm{MeV} \tag{8}$$

with $\chi = 0$, 1, or 2 for odd-odd, odd-even, or even-even nuclei, respectively.

The nuclear level-density parameter is a function of Z, N, and $E^\star$ of the corresponding nucleus [47–49]:

$$a(Z,N,E^\star) = \tilde{a}(A)\left\{1 + \delta W_\mathrm{gs}(Z,N)\frac{f(E^\star - \Delta)}{E^\star - \Delta}\right\}, \tag{9}$$

where

$$f(E) = 1 - \exp(-\gamma E); \tag{10}$$

$$\tilde{a}(A) = \alpha A + \beta A^{2/3} B_\mathrm{s} \tag{11}$$

is the asymptotic Fermi-gas value at high excitation energies, and $\delta W_\mathrm{gs}(Z,N)$ is the shell correction in the nuclear-mass formula. The coefficients α and β correspond to the volume and surface components, which, along with γ, are taken to be phenomenological constants. We use the values $\alpha = 0.114$, $\beta = 0.098$, and $\gamma = 0.051$ (all in MeV^{-1}), corresponding to the first set of systematics given in table 3 of ref. [49], which includes the shell corrections of ref. [50]. B_s is the surface area of the nucleus in units of the surface for a sphere of equal volume. $B_\mathrm{s} \approx 1$ for nearly spherical nuclei with small deformation. Since the surface is systematically larger at the saddle point, $B_\mathrm{s} > 1$ there; in fact $B_\mathrm{s} \approx 2^{1/3} \approx 1.26$ for the configuration corresponding to the splitting of the compound nucleus into two equal spherical fragments. Such a case nearly corresponds to the fission of low-fissility nuclei, while for highly fissile nuclei the shape at the saddle point is closer to a sphere and $B_\mathrm{s} \approx 1$.

In ref. [52], for example, the level-density parameter a_f at the fission saddle point (in the transition state) is calculated using an analogous parameter for the neutron emission channel a_n. In this way, a constant ratio $r = a_\mathrm{f}/a_n$ is assumed and used as a fitting parameter of the model. As a consequence of this assumption, the shell effect influence on the level density for the neutron emission channel is transferred to the level density at the saddle point. However, contrary to ref. [52], we expect that the shell corrections at the saddle point with large deformation have no relation to those at the ground state with relatively small equilibrium deformation [29,47,48]. We conclude that the shell corrections should be much smaller at the saddle point and therefore we can use the asymptotic value $\tilde{a}_\mathrm{f}(A)$ instead of an energy-dependent $a_\mathrm{f}(Z,N,E^\star)$. The value of $\tilde{a}_\mathrm{f}(A)$ is assumed to be proportional to the asymptotic one for the neutron emission channel $\tilde{a}_n(A)$.

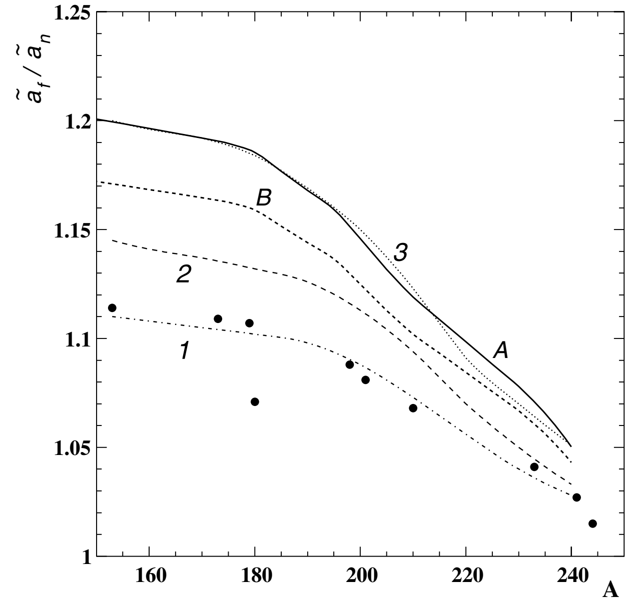

Fig. 5. The closed circles are the $\tilde{a}_\mathrm{f}/\tilde{a}_n$ ratios calculated in ref. [53] based on the liquid-drop model and the dot-dashed curve marked "1" shows the result of our interpolation of these discrete ratios. The two sets, $\mathcal{A}$ and $\mathcal{B}$, of $\tilde{a}_\mathrm{f}/\tilde{a}_n$ values used in our calculations are represented by the solid and short-dashed curves, respectively. For comparison, calculational results from refs. [54,55] are shown by the long-dashed and dotted curves marked as "2" and "3," respectively.

The ratios $\tilde{a}_\mathrm{f}/\tilde{a}_n$ for some nuclei were calculated in ref. [53] based on the liquid-drop model [56] and using an expression similar to eq. (11), but with an additional curvature term. As shown in fig. 5, the ratios obtained from this procedure are very close to unity for the actinides ($\sim$ 1.02–1.04) and are higher for the preactinides ($\sim$ 1.07–1.12). Since the value for $\tilde{a}_\mathrm{f}/\tilde{a}_n$ used in our calculations needs to be valid for a much wider range of nuclides, we tried to interpolate between the values tabulated in ref. [53] to obtain the values for other nuclei as shown, for example, in fig. 4. Such a procedure deals with the average values of $\tilde{a}_\mathrm{f}/\tilde{a}_n$ and neglects possible rapid changes of the ratio for individual isotopes. However, this is the only method to estimate $\tilde{a}_\mathrm{f}/\tilde{a}_n$ for the region of nuclei between Po and Th, where experimental information on the nuclear level densities is lacking.

Using this interpolation procedure, we find that the photofission cross-sections for lead are underestimated by theory by a large factor. Therefore, to improve the agreement with the experimental data [2,4], we increased the difference between the values of ref. [53] and unity by a factor of 1.7 (variant $\mathcal{A}$) or 1.5 (variant $\mathcal{B}$). The resulting curves are shown in fig. 5. As one can see, such modification is not too far outside the range of $\tilde{a}_\mathrm{f}/\tilde{a}_n$ values which were obtained in refs. [53–55]. Moreover, the curve of variant $\mathcal{A}$ independently obtained from the analysis of the photofission data on $^\mathrm{nat}$Pb [2,4], agrees very well indeed with the values of ref. [55], the most recent and comprehensive of these studies of nuclear level densities, denoted by curve "3" in fig. 5.

Following refs. [47–49], the fission barriers are computed from the macroscopic liquid-drop component $B_\mathrm{LD}(Z,N)$ and the shell correction at the nuclear ground state $\delta W_\mathrm{gs}(Z,N)$ [50]:

$$B_\mathrm{f}(Z,N,E^\star) = B_\mathrm{LD}(Z,N) - \delta W_\mathrm{gs}(Z,N). \qquad (12)$$

In this expression, the shell correction at the saddle point is neglected.

The validity of the above-mentioned assumptions (except for our interpolation procedure for $\tilde{a}_\mathrm{f}/\tilde{a}_n$) was confirmed in previous studies of nuclear fission induced by various projectiles. For example, the dependence of W_f on the target nucleus mass for reactions with stopped π^- mesons, photons, protons, and α-particles with kinetic energies below 1 GeV was considered in ref. [29] within the framework of the intranuclear cascade, fission, and evaporation models. The calculated values were compared with the experimental data available at that time. The influences on fission probability of shell effects, preequilibrium emission from the residual nucleus, and the parameters of the liquid-drop model were studied. Later, the W_f values were deduced within this model for heavy nuclei ($Z^2/A > 30$) in reactions with these projectiles and with pions in flight [30].

2.4 Results for electromagnetically induced heavy-ion fission

As shown above, when energetic photons are absorbed by heavy nuclei, a wide range of excited residual nuclei is created, having masses and charges far from the stability line. Beams of relativistic radioactive nuclei provide new access to fission studies of such nuclei. For example, in ref. [57], fission of 58 secondary projectiles ($^{231-234}$U, $^{226-231}$Pa, $^{221-229}$Th, $^{215-226}$Ac, $^{211-223}$Ra, $^{208-212,217,218}$Fr, $^{205-209}$Rn, and ^{205,206}At) produced by fragmentation of 1 GeV/nucleon ^{238}U nuclei has been studied. The total fission cross-section in secondary collisions of these nuclei with a lead target at energy 420 MeV/nucleon was found to consist of two comparable parts, due to hadronic and electromagnetic interactions.

Electromagnetically induced fission results from absorption of virtual photons. According to the RELDIS model, which is based on the Weizsäcker-Williams method of equivalent quanta, such nuclei are typified by low excitations, $\langle E^\star\rangle \sim$ 12–13 MeV, due to the photons in the GDR region with energies below 20 MeV. The recent data [57] make possible a crucial test of the model, since $E^\star \sim B_\mathrm{f}$ in such processes. This makes the model results very sensitive to the fission barrier shape and height, as well as to the level-density parameterization $\rho(E^\star)$ used in the calculations.

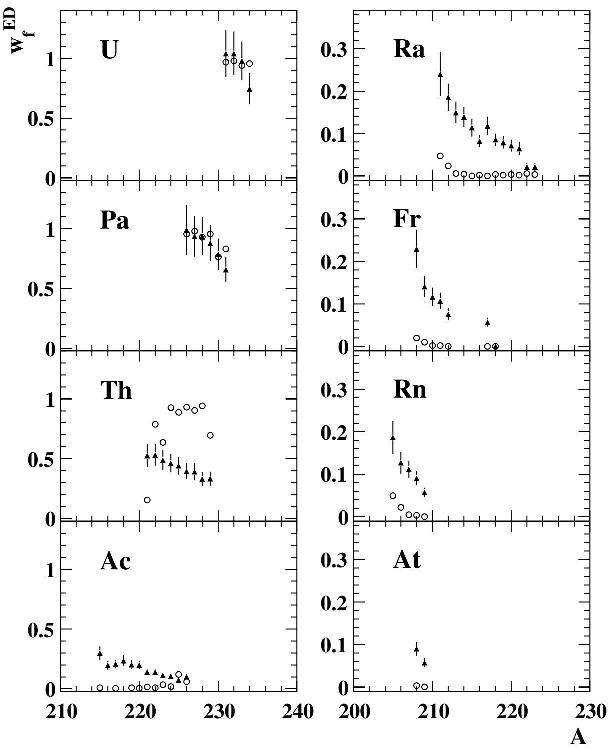

Fig. 6. Fission probabilities in electromagnetic dissociation of heavy ions at 420 MeV/nucleon on a lead target. Experimental fission probabilities extracted from the fission cross-section of ref. [57] are shown by the full triangles. Calculational results are given by the open circles.

The experimental fission probabilities w_f^ED for each of the ions were derived by dividing the measured fission cross-sections of ref. [57] by the calculated total electromagnetic-dissociation cross-sections σ^ED. The calculations were performed by accounting for absorption of either one or two photons in each collision event; see refs. [12–14] for details. Double-photon absorption processes were taken into account by applying the harmonic-oscillator ansatz in conjunction with the folding model [58].

Since experimental data on the total photoabsorption cross-sections for unstable nuclei are not available, the cross-sections for nearby stable nuclei were used in calculations of σ^ED. Approximations of the total photoabsorption cross-sections obtained in ref. [59] were used. Such a substitution generally leads to 2–3% uncertainty in σ^ED according to the estimates based on the GDR sum rule [59,60].

Experimental and calculated values of w_f^ED are shown in fig. 6. Very good agreement is found for the most fissile nuclei $^{231-234}$U and $^{226-231}$Pa. The description of the data for Th nuclei is poor. The calculated values for Ac, Ra, Fr, Rn, and At are much lower than the experimental data, but good agreement is obtained for the values of w_f^ED for those isotopes which are closest to the stable isotopes of Ac, Ra, and Fr. This is explained by the fact that the input calculational parameters were adjusted to describe the fission of nuclei close to the stability line. The calculations

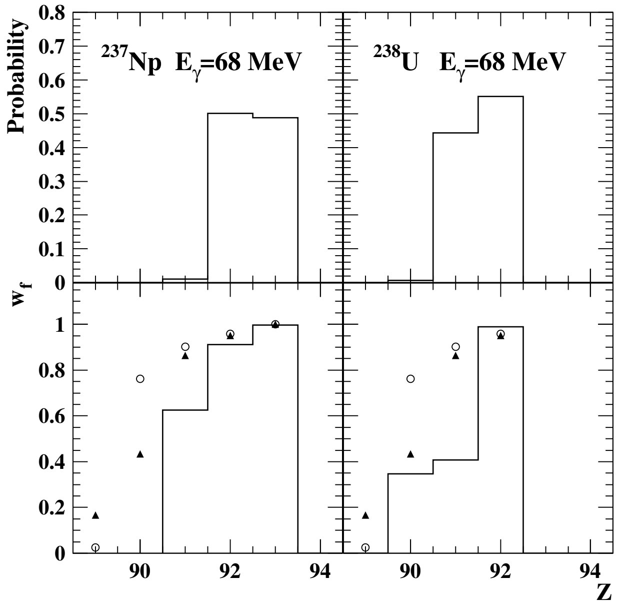

Fig. 7. Top: charge distributions of residual nuclei created in photoabsorption on ^{237}Np and ^{238}U at $E_\gamma = 68$ MeV. Bottom: fission probabilities for such nuclei. Calculated fission probabilities in photoabsorption at $E_\gamma = 68$ MeV are shown by histograms. Calculated and measured fission probabilities for heavy ions at 420 MeV/nucleon are shown by open circles and filled triangles, respectively.

presented in ref. [57] for Ra nuclei also underestimate the electromagnetic-fission cross-sections. At the present time, the description of the fission of radioactive nuclei seems to present a common difficulty to all fission models. Further work on our fission model should be aimed at a better description of the fission of unstable nuclei.

Using single-humped fission barriers instead of double-humped barriers and neglecting the collective effects in the nuclear level-density formula does not lead to disagreement with the data for U and Pa nuclei. Below we estimate how the failure to describe the fission of other radioactive nuclei may affect the total calculated fission probability W_f in phototoabsorption. The 58 radioactive nuclei listed are only a small subset of all of the residual nuclei created in photoabsorption of GeV photons. As a rule, such residual nuclei are much more highly excited. However, photoabsorption at lower energies, such as at $E_\gamma = 68$ MeV, creates nuclei with $\langle E^\star \rangle$ of only about 20 MeV, much closer to nuclei with $\langle E^\star \rangle \sim$ 12–13 MeV, which is the case for electromagnetically induced heavy-ion fission. This makes useful the comparison presented in fig. 7.

The charge distributions of residual nuclei created in photoabsorption on ^{237}Np and ^{238}U at $E_\gamma = 68$ MeV are shown in fig. 7, together with the calculated fission probabilities for residual elements. Excited Np, U, Pa, and Th nuclei are created in photoabsorption at this energy. The calculated and measured values of w_f^ED for such nuclei in electromagnetically induced fission are shown in the bottom part of the same plot. These values are obtained as average values of the points for individual nuclides, and they are different from the values of w_f for photofission, due to the difference in $E^\star$. As shown, fission probability in electromagnetically induced fission of U and Pa is described at the 5% level of accuracy. The agreement for Th is poor, but this element is less abundant in the ensembles of residual nuclei; the estimate of the total fission probability W_f for the whole ensemble is quite reliable.

The reliability of the fission model can be quantitatively assessed by calculating the total fission probability for the ensembles presented in fig. 7. In the following two hypothetical examples, the experimental and theoretical values for w_f^ED were used, but in both cases the residual-element abundances were taken for photoabsorption at $E_\gamma = 68$ MeV. As found for the γ + Np case, $W_\mathrm{f} = 0.98$ for the calculated w_f^ED, compared with $W_\mathrm{f} = 0.97$ for the value extracted from experiment. For the γ + U case, $W_\mathrm{f} = 0.93$ and $W_\mathrm{f} = 0.91$, respectively, for the two sets of input w_f^ED values. Therefore, the failure to describe the fissility of Th leads to an error in W_f of only $\sim 3\%$. In this way, the reliability of the fission model is demonstrated for the most fissile and most probable residual nuclei created in photoabsorption on ^{237}Np and ^{238}U at low energies.

3 Results and discussion

3.1 Fission probabilities for ^{237}Np, ^{233,235,238}U, ^{232}Th, and $^{\mathrm{nat}}$Pb

As a rule, the liquid-drop model predicts proton-rich nuclei to have higher probability to undergo fission [50,56]. The probability w_f for a residual nucleus with given mass A_RN and charge Z_RN to undergo fission during the last stage of the reaction is shown in fig. 8 for $E_\gamma = 3.77$ GeV for ^{237}Np, ^{238}U, and ^{232}Th.

The probability w_f is defined for each of the nuclides created after the INC stage of photoabsorption, while the fission probability W_f refers to the appropriately weighted average value calculated over the whole ensemble of residual nuclei. For example, w_f turns out to be below 0.2 for some regions of A_RN and Z_RN far from the A and Z of the initial target nucleus. However, these regions do not contribute much to the resulting W_f, since the probability to create a nucleus with such A_RN and Z_RN is low, as can be seen in figs. 4 and 8. As a result, the W_f values, shown in fig. 9 as functions of E_γ for ^{237}Np, ^{238}U, and ^{232}Th, are generally above 0.6 despite the fact that some of the residual nuclei have a low probability w_f to undergo fission. As is also shown in fig. 9, this is true for ^{233}U and ^{235}U as well, for which $0.8 \leq W_\mathrm{f} \leq 0.95$, almost as large as the corresponding values for ^{237}Np.

Our calculated values for W_f for $^{\mathrm{nat}}$Pb are much lower, $\sim$ 0.10–0.15, as can be seen in fig. 9 as well. The values for W_f are first obtained for each of the most abundant lead isotopes, ^{206}Pb (24.1%), ^{207}Pb (22.1%), and ^{208}Pb (52.4%), and then are averaged with appropriate weights to obtain the fission probability for $^{\mathrm{nat}}$Pb.

As can be seen in fig. 9, two extreme cases are represented by photoabsorption on the highly fissile actinides

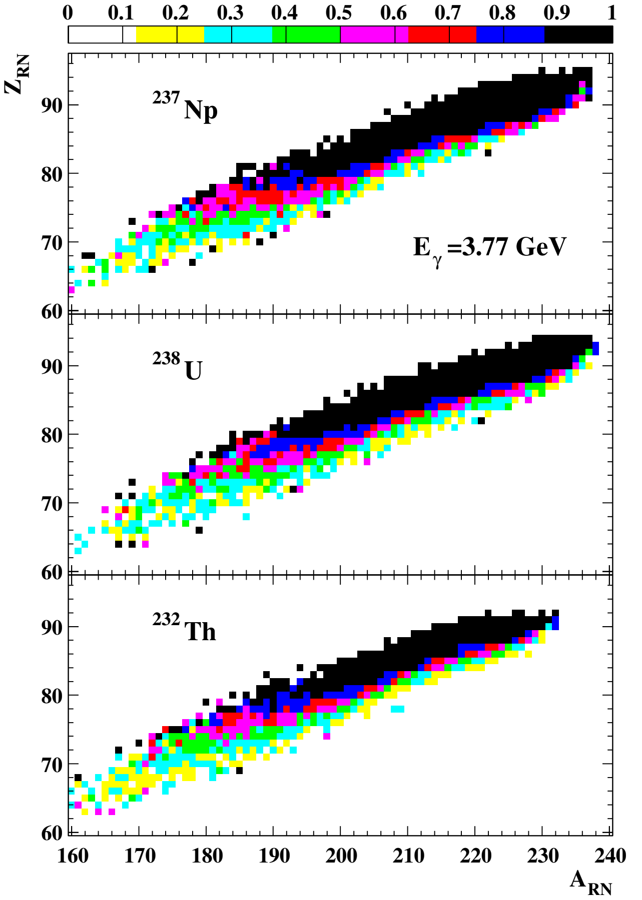

Fig. 8. Fission probabilities w_f of each of the residual nuclei created after the fast stage of the photoabsorption process for $E_\gamma = 3.77$ GeV on ^{237}Np, ^{238}U, and ^{232}Th (top, middle, and bottom panels, respectively).

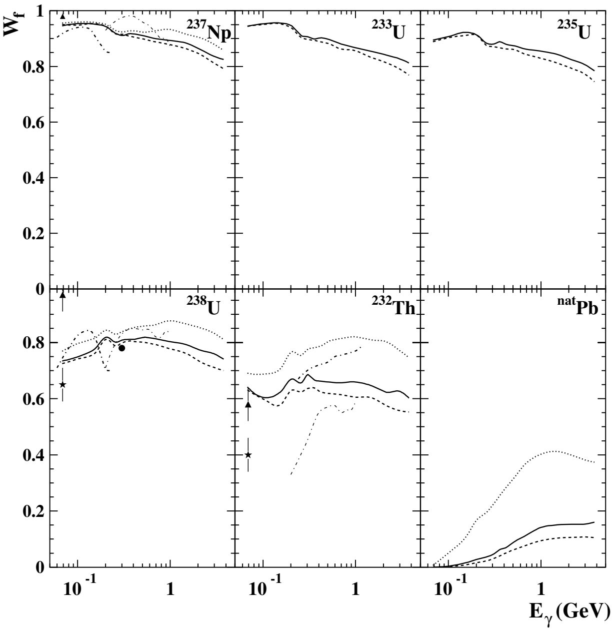

Fig. 9. Fission probabilities W_f for photoabsorption in ^{237}Np, ^{233}U, ^{235}U, ^{238}U, ^{232}Th, and $^{\mathrm{nat}}$Pb. Our calculated results for variants $\mathcal{A}$ and $\mathcal{B}$ are given by the solid and dashed lines, respectively; variant $\mathcal{A}$ without pre-equilibrium emission is represented by the dotted lines. Earlier calculational results for ^{237}Np, ^{238}U, and ^{232}Th [35] are given by thin dot-dashed lines; for ^{237}Np, ^{238}U [26], and for ^{232}Th [61] are given by thick dot-dashed lines. The circle represents the calculational result of ref. [62]. Values inferred in ref. [52] from the old experimental data of refs. [21,52] are given by the triangles and stars, respectively.

^{237}Np, ^{233}U, and ^{235}U and on the preactinide $^{\mathrm{nat}}$Pb. At $E_\gamma = 68$ MeV, fission clearly dominates for the residual nuclei created after photoabsorption on ^{237}Np, ^{233}U, and ^{235}U. However, the fission contribution gradually decreases with increasing E_γ, since, on average, a wider distribution of residual nuclei created at higher E_γ has lower fission probability and nucleon evaporation becomes more important. A completely different tendency is found for the photofission of lead, which has a clear threshold behavior. Due to high fission barriers for the residual nuclei created after photoabsorption on $^{\mathrm{nat}}$Pb, the fission process is suppressed below $E_\gamma \sim 100$ MeV and only evaporation from excited nuclei can take place there. Above $E_\gamma \sim 100$ MeV, the fission probability W_f gradually increases to $W_\mathrm{f} \sim 0.1$, but this still represents only a small part of the de-excitation process. An intermediate tendency is found in photoabsorption on ^{238}U and ^{232}Th. For these cases, W_f has a very broad maximum at $E_\gamma \sim 0.5$–1 GeV and decreases gradually with E_γ above ~ 1 GeV.

Different mechanisms of photoabsorption play a role at different photon energies. As a result, a variation in the trend of the average excitation energy *versus* E_γ is found for 180–250 MeV, as seen in fig. 1. The variations of $W_\mathrm{f}(E_\gamma)$ which are seen in fig. 9 have the same origin. The probability for a pion produced in the $\gamma N \to \pi N$ process to be absorbed in the nuclear medium increases rapidly with E_γ as one approaches the region of the $\Delta_{33}(1232)$-resonance, $E_\gamma \sim 200$–500 MeV. If this pion is re-absorbed in the nucleus, the excitation energy increases and, therefore, so does the fission probability.

If the pre-equilibrium emission process after the cascade stage of the photonuclear reaction is neglected in the calculations, the decay of the excited compound nucleus takes place with higher excitation energy $E^\star$ and fissility parameter Z^2/A. This generally leads to higher values of W_f, as shown in fig. 9 by dotted lines for ^{237}Np, ^{238}U, ^{232}Th, and $^{\mathrm{nat}}$Pb.

The changes in W_f due to the variation of $\tilde{a}_\mathrm{f}/\tilde{a}_n$ ($\mathcal{A}$ and $\mathcal{B}$) are of the order of 5% for ^{237}Np, ^{233}U, ^{235}U, and ^{238}U and 10% for ^{232}Th, as also can be seen in fig. 9. This important observation of the relative stability of the calculated W_f is true for actinide nuclei only. This makes it possible to infer the total photoabsorption cross-section from the photofission data [1,3,4] and the calculated values for W_f.

Fission probabilities estimated in refs. [21,52] from previous experimental data on absolute photofission cross-sections are given in fig. 9 for comparison, although they are in poor agreement with each other. The calculated W_f

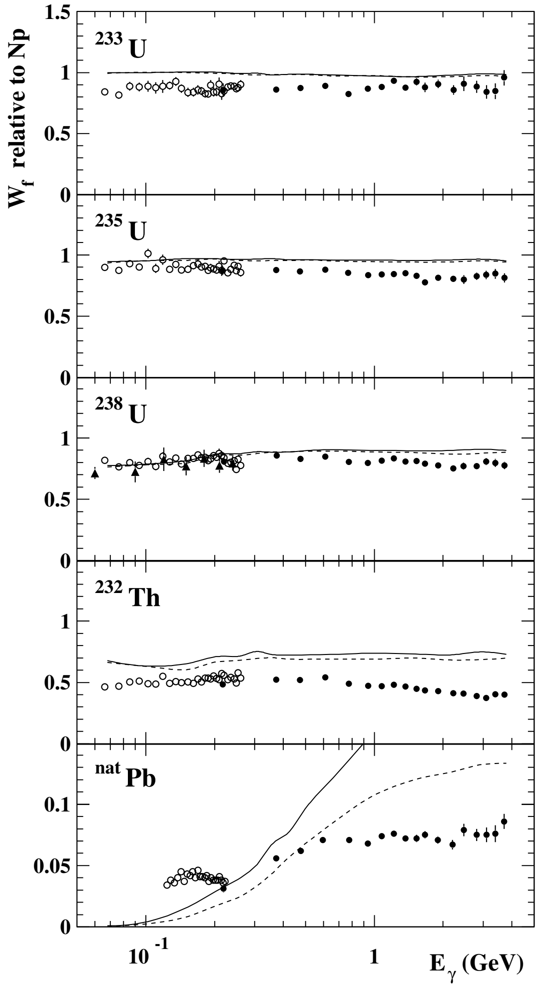

Fig. 10. Fission probabilities relative to ^{237}Np for photoabsorption in ^{233}U, ^{235}U ^{238}U, ^{232}Th, and ^{nat}Pb. Our calculated results for variants $\mathcal{A}$ and $\mathcal{B}$ are given by the solid and dashed lines, respectively. The open and closed circles represent the data from SAL [1,2] and JLab [3,4], respectively. The Novosibirsk data [26,27] for the ^{238}U-to-^{237}Np ratio are shown by the closed triangles.

value from ref. [62] is in good agreement with our results for ^{238}U.

Compared with the approach of refs. [49,26], several simplifications were adopted in our fission calculations. For example, we do not use double-humped fission barriers for actinides, nor do we take into account any collective effects in the nuclear level-density formula because i) information (either experimental or theoretical) on such effects is not available for the whole range of residual nuclei, and ii) at high excitation energies ($E^\star \geq 30$ MeV), which are our interest here, the fission probability W_f is sensitive mainly to the ratio $\tilde{a}_\mathrm{f}/\tilde{a}_n$. The uncertainty in the choice of $\tilde{a}_\mathrm{f}/\tilde{a}_n$ exceeds the uncertainties resulting from the selection of other calculational parameters describing the decay of the excited residual nucleus.

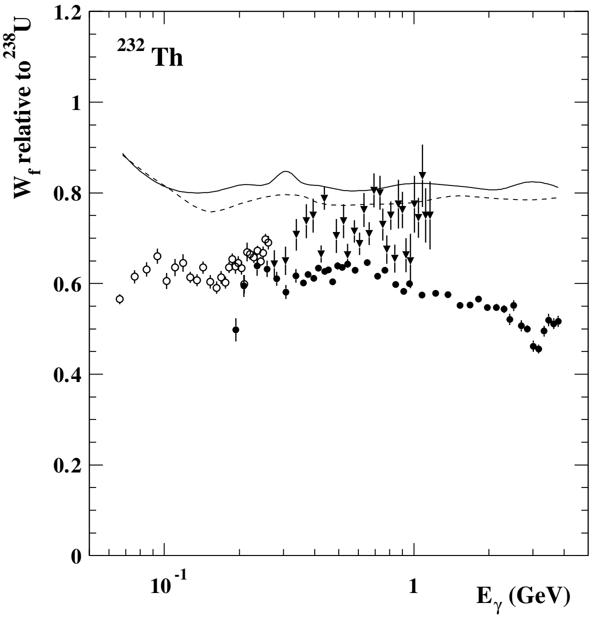

Fig. 11. ^{232}Th fission probability relative to ^{238}U. Our calculated results for variants $\mathcal{A}$ and $\mathcal{B}$ are given by the solid and dashed lines, respectively. The open and closed circles represent the data from SAL [1,2] and JLab [3,4], respectively. The data of ref. [61] are shown by the closed triangles.

As shown in fig. 9, the difference between our approach and that of refs. [26,49] does not lead to a dramatic difference in W_f for ^{237}Np and ^{238}U. In the limited energy region $60 \leq E_\gamma \leq 240$ MeV, $W_\mathrm{f} \sim 85$–95% and ~ 70–85%, respectively, for both approaches. However, for $250 \leq E_\gamma \leq 1200$ MeV, our fission probabilities for ^{232}Th (variants $\mathcal{A}$ and $\mathcal{B}$) are noticeably lower than those of ref. [61], where the effect of pre-equilibrium emission, the trawling effect, and some multiple-pion photoproduction channels were neglected.

Our calculated fission probabilities relative to ^{237}Np are shown in fig. 10 for the uranium isotopes, thorium, and lead as a function of E_γ, compared with the experimental data from SAL [1,2] and JLab [3,4]. The data from [26, 27] for ^{238}U-to-^{237}Np ratio, also shown in fig. 10, are in good agreement with the SAL and JLab data. Again, only minor changes are found due to the choice of $\tilde{a}_\mathrm{f}/\tilde{a}_n$ in variants $\mathcal{A}$ and $\mathcal{B}$ for actinides, whose energy dependence of relative fission probabilities is flat.

A better description of the experimental fission probabilities relative to ^{237}Np is found for ^{233}U, ^{235}U, and ^{238}U. Larger uncertainties in the calculations exist for ^{232}Th, and especially for ^{nat}Pb, where the W_f values are farther from unity.

As shown in figs. 9 and 10, our calculated fission probabilities for ^{237}Np and ^{238}U are in agreement within $\sim$ 10–20% with the theoretical results of other authors and the estimates based on earlier experimental data from the literature, which are available mainly at low energies, $E_\gamma < 300$ MeV. The fission probabilities for ^{237}Np and ^{233,235,238}U are stable within $\sim$ 7% with respect to the choice of calculational parameters. At $E_\gamma \geq 100$ MeV, the main uncertainty in our results for these nuclei is due to the choice of $\tilde{a}_\mathrm{f}/\tilde{a}_n$.

For the case of ^{232}Th, we see a larger discrepancy with the SAL [1,2] and JLab [3,4] data than for the other actinides, while the energy dependence is still reproduced reasonably well. The fissility of ^{232}Th relative to ^{238}U is shown in fig. 11. A discrepancy between theory and experiment exists also for this ratio. It should be noted, however, that the agreement between the recent data [1–4] and earlier results [61] is poor, while theoretical results are found to be closer to the earlier data [61].

The ^{232}Th nucleus deviates from the pattern common to the heavier actinides at lower energies with regard to fission probability [18] and the number of prompt neutrons emitted per fission [19] because it has a more spherical shape [18]. It may be that this deviation persists to GeV energies as well.

3.2 Absolute photofission cross-sections for ^{237}Np, ^{233,235,238}U, ^{232}Th, and $^{\mathrm{nat}}$Pb

In order to obtain the absolute photofission cross-section, the calculated fission probability must be multiplied by the total photoabsorption cross-section. In the RELDIS code, the values of the total photoabsorption cross-section are taken from approximations to the existing experimental data. In the GDR region, the Lorentz-curve fits with parameters from refs. [59,60], corrected according to the prescription of ref. [63], were used for this purpose. Above the GDR region, where quasideuteron absorption becomes dominant, the total cross-section is taken from the estimate of ref. [42] (based on the quasideuteron model [41].)

Above the pion production thresholds, a "universal" behavior, $\sigma_{\gamma A}(E_\gamma) \propto A$, is observed (see refs. [24,25] for the latest experimental data). This means that the total photoabsorption cross-section per bound nucleon $\sigma_{\gamma A}(E_\gamma)/A$ has the same magnitude and the same energy dependence for light, medium, and heavy nuclei (C, Al, Cu, Sn, and Pb) at least up to $E_\gamma \sim 3$ GeV. Therefore, having the data for one nucleus, one can calculate the cross-section for other nuclei. However, in this energy region the Universal Curve $\sigma_{\gamma A}(E_\gamma)/A$ is very different from the values extrapolated from the cross-sections on free nucleons, $(Z\sigma_{\gamma p} + N\sigma_{\gamma n})/A$, which are deduced from proton [64,65] and deuteron data [66]. For $E_\gamma > 3$ GeV, the universal behavior breaks down, and, for example, the ratio $\sigma_{\gamma A}(E_\gamma)/A$ for lead is 20–25% lower than for carbon [67] due to the nuclear shadowing effect [68,69]. In order to approximate the total photonuclear cross-sections at $E_\gamma > 3$ GeV, we use recent results for $\sigma_{\gamma A}(E_\gamma)/A$ obtained with the Glauber-Gribov approximation within the Generalized Vector Dominance Model (see ref. [67] and references therein).

Our calculated absolute photofission cross-sections for ^{237}Np, ^{233,235,238}U, ^{232}Th, and $^{\mathrm{nat}}$Pb are shown in fig. 12 and compared with the experimental data of refs. [1–4]. For ^{237}Np and ^{233,235,238}U, variants $\mathcal{A}$ and $\mathcal{B}$ give consistent results. Except for ^{232}Th, neglecting pre-equilibrium emission after the INC stage does not lead to a large change in the calculated photofission cross-section; a small increase in the calculated cross-section is obtained only for $E_\gamma \gtrsim 1$ GeV. When normalized to the "Universal Curve" in this way, our calculated absolute cross-sections agree within $\sim 7\%$ with the data for ^{233}U and ^{235}U, but are underestimated for ^{237}Np and ^{238}U and overestimated for ^{232}Th, especially in the $\Delta_{33}(1232)$-resonance region, although qualitative agreement for the shape of the cross-sections is found. It should be stressed, however, that these cross-sections were calculated using "the universal" $\sigma_{\gamma A}(E_\gamma)/A$ dependence, which was obtained for nuclei with $A \leq 208$.

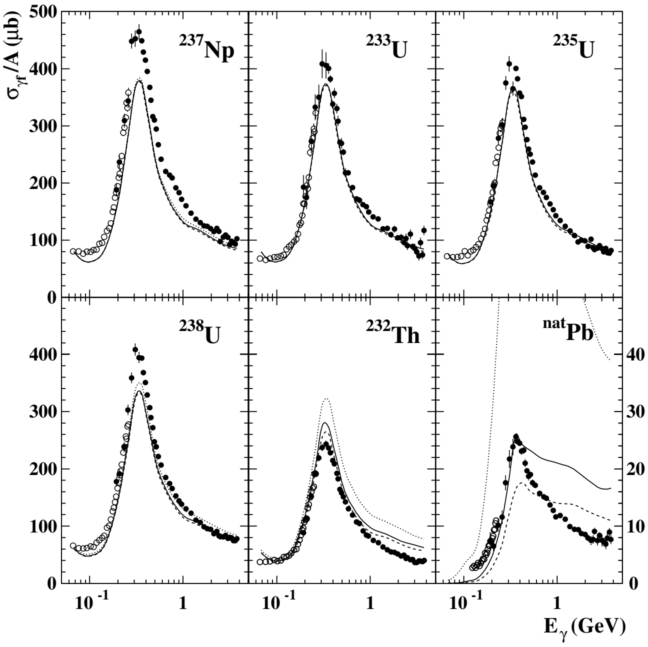

Fig. 12. Absolute photofission cross-sections per bound nucleon for ^{237}Np, ^{233,235,238}U, ^{232}Th, and $^{\mathrm{nat}}$Pb. Our calculated results for variants $\mathcal{A}$ and $\mathcal{B}$ are given by the solid and dashed lines, respectively. Variant $\mathcal{A}$ without pre-equilibrium emission is represented by the dotted lines. Cross-section values given in the plot for $^{\mathrm{nat}}$Pb (only) are shown on a separate scale on the right-hand side. The data are from refs. [1–4].

Using the same procedure, we obtain the absolute photofission cross-section for $^{\mathrm{nat}}$Pb shown in fig. 12 on a separate scale, since this cross-section was found to be much smaller than those for the actinides. Although the results of the calculation based on set $\mathcal{A}$ for the $\tilde{a}_{\mathrm{f}}/\tilde{a}_n$ ratios are adjusted to match the data near the peak of $\Delta_{33}(1232)$, at higher energies they grossly overestimate the photofission cross-section. Moreover, neglecting pre-equilibrium emission leads to a large increase of the fission probability due to the increase of the excitation energy of the compound nucleus. This leads to an unreasonably large enhancement of the fission channel. Since our study is aimed mainly at photofission reactions in the actinide region, we did not attempt to obtain better agreement with the photofission cross-section for $^{\mathrm{nat}}$Pb via further adjustment of the calculational parameters for each stable isotope of lead or by introducing an empirical dependence of fission barriers on $E^\star$, as was done in refs. [70–72].

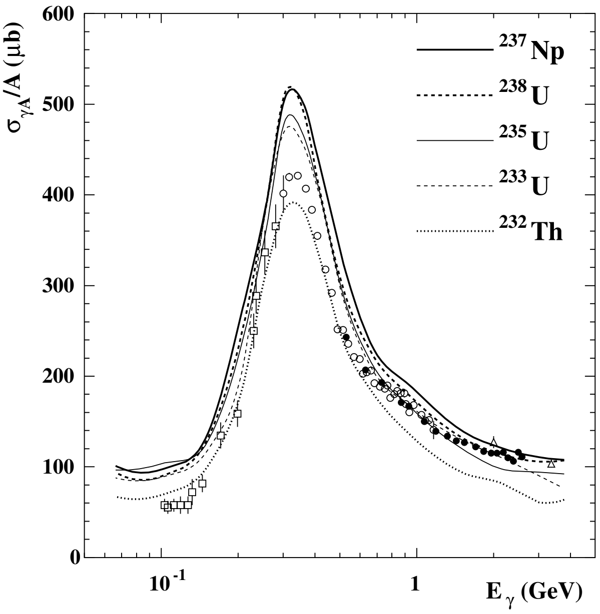

Fig. 13. Total photoabsorption cross-section per bound nucleon for actinide nuclei evaluated from the photofission data of refs. [1,4] and our calculated fission probabilities. Average data for C, Al, Cu, Sn, and Pb are shown by the open [24] and closed [25] circles. Typical values of the systematic uncertainties for the measurements of ref. [24] are shown for the first and last points. Additional experimental data for ^{238}U above 2 GeV [73] and for Pb below 0.3 GeV [42,74–76] are shown by the open triangles and squares, respectively.

It has been suggested [22,23,77] that one might be able to infer the photoabsorption cross-section from the measured photofission cross-section for very heavy nuclei. In this manner, the behavior of the "Universal Curve" for such nuclei could be investigated. We can calculate the total photoabsorption cross-section per bound nucleon $\sigma_{\gamma A}(E_\gamma)/A$ by means of our calculated values for $W_{\mathrm{f}}(E_\gamma)$ and the actinide photofission cross-section data of refs. [1,4], using

$$\frac{\sigma_{\gamma A}(E_\gamma)}{A} = \frac{\sigma_{\gamma \mathrm{f}}(E_\gamma)}{A}\frac{1}{W_{\mathrm{f}}(E_\gamma)}. \qquad (13)$$

The data for each of the target nuclei used in refs. [1,4], except for $^{\mathrm{nat}}$Pb, were interpolated by smooth curves and then divided by the calculated W_{f}. The results of this procedure, shown in fig. 13, are in agreement within $\sim 10\%$ of each other, except for ^{232}Th. Those for ^{232}Th are obtained with $W_{\mathrm{f}}(E_\gamma)$ values that we found to be more sensitive to the choice of calculational parameters and hence less accurately defined. Reasonable agreement is found with the $\sigma_{\gamma A}(E_\gamma)/A$ data of refs. [24,25,73] at $E_\gamma \geq 0.7$ GeV, but marked disagreement in strength ($\sim 20\%$) exists in the Δ region. However, the combined uncertainties arising from both the experimental data and the theoretical calculations presented in this paper are large enough to cast reasonable doubt on any further conclusions that might be inferred from the total photoabsorption cross-section curves shown in fig. 13.

4 Conclusions

We have calculated, using the RELDIS model, the fission probabilities of ^{237}Np, ^{233,235,238}U, ^{232}Th, and $^{\mathrm{nat}}$Pb as a function of incident-photon energy. We have used these values, together with the total photoabsorption cross-sections inferred from previous data on lighter nuclei, to obtain absolute photofission cross-sections to be compared with the measured photofission cross-sections from SAL and JLab. We also have attempted to use these values, together with the data from SAL and JLab, to infer the total photoabsorption cross-sections for these nuclei. We now answer the questions raised in sect. 1.3.

1) We have been able to describe the photofission of the actinide nuclei over a very broad energy range. The calculated fission probabilities for ^{237}Np, ^{238}U, ^{235}U, and ^{233}U were found to be stable within 7% with respect to reasonable changes of the input calculational parameters.
2) Our model calculations show that photonuclear reactions become more complex in the GeV energy region, when many reaction channels are open. Contrary to the naive expectation that for the actinides, the higher the photon energy, the closer the fission probability W_{f} should be to unity, our calculated fission probabilities for $E_\gamma > 1$ GeV are found not to exceed those values for $E_\gamma \sim$ 50–100 MeV; they are, in fact, predicted to decrease somewhat. At higher photon energies, only a small part of the energy is converted into the internal excitation of the absorbing nuclear system. The resulting behavior of W_{f} is due to the creation of compound nuclei with fissility parameter Z^2/A much lower than that for the target nucleus.
3) We show that the residual nuclei after direct and preequilibrium emission of hadrons resemble the target nucleus, in the sense that the fissility parameter Z^2/A is similar, only for relatively low incident-photon energies ($E_\gamma \leq 100$ MeV). They differ markedly for GeV energies. The products of photospallation reactions have relatively low probabilities to undergo fission, but high rates to decay via the less collective channels leading to the evaporation of nucleons.
4) Our calculations show that for the actinides, fission is not the only significant outcome following photoabsorption at GeV energies. Even at the highest tagged-photon energies ($E_\gamma \sim 4$ GeV) used in the measurements at JLab, the competition with the evaporation process is still important. Therefore, we conclude that the photofission cross-section cannot be substituted for the total photoabsorption cross-section in the GeV energy region, even for those nuclei with the largest fissility parameters. Either the previous total photoabsorption data on lighter nuclei must be extended to the actinides to obtain the absolute photofission cross-sections or the measured photofission cross-sections must be combined with calculated fission probabilities to obtain the total photoabsorption cross-sections. Either way, serious discrepancies are seen in figs. 12 and 13.

5) The calculational uncertainties for fission probabilities for Np and U are estimated to be at the level of 10%, which should be combined with the $\sim 5\%$ accuracy of the measured photofission cross-sections or with the accuracy of previous measurements of the "Universal Curve," which can be estimated as no better than 5% as well. These uncertainties taken together prevent us from drawing a definitive conclusion that the "Universal Curve," obtained for nuclei with $A \leq 208$, breaks down for heavy nuclei with $A \geq 233$ and for E_γ in the $\Delta_{33}(1232)$-resonance region. Thus, our findings demonstrate once again (see ref. [4]) the need for direct measurement of the total photoabsorption cross-sections for the heavy actinides.

I.A.P. thanks the Center for Nuclear Studies of The George Washington University for warm hospitality and financial support and the Russian Foundation for Basic Research for support in part under Grant RFFI-02-02-16013. This work is supported by the US Department of Energy under Grant DE-FG02-95ER40901.

References

1. J.C. Sanabria, B.L. Berman, C. Cetina, P.L. Cole, G. Feldman, N.R. Kolb, R.E. Pywell, J.M. Vogt, V.G. Nedorezov, A.S. Sudov, G.Ya. Kezerashvili, Phys. Rev. C **61**, 034604 (2000).
2. J.C. Sanabria, PhD Thesis, The George Washington University (1999).
3. C. Cetina, B.L. Berman, W.J. Briscoe, P.L. Cole, G. Feldman, P. Heimberg, L.Y. Murphy, S. Philips, J.C. Sanabria, Hall Crannell, A. Longhi, D.I. Sober, G.Ya. Kezerashvili, Phys. Rev. Lett. **84**, 5740 (2000).
4. C. Cetina, P. Heimberg, B.L. Berman, W.J. Briscoe, G. Feldman, L.Y. Murphy, Hall Crannell, A. Longhi, D.I. Sober, J.C. Sanabria, G.Ya. Kezerashvili, Phys. Rev. C **65**, 044622 (2002); C. Cetina, PhD Thesis, The George Washington University (2001).
5. J. Ahrens, J. Arends, P. Bourgeois, P. Carlos, J.L. Fallou, N. Floss, P. Garganne, S. Huthmacher, U. Kneissl, G. Mank, B. Mecking, H. Ries, R. Stenz, A. Veyssière, Phys. Lett. B **146**, 303 (1984).
6. A.S. Iljinov, M.V. Kazarnovsky, E.Ya. Paryev, *Intermediate Energy Nuclear Physics* (CRC Press, Boca Raton, 1994).
7. A.S. Iljinov, I.A. Pshenichnov, N. Bianchi, E. De Sanctis, V. Muccifora, M. Mirazita, P. Rossi, Nucl. Phys. A **616**, 575 (1997).
8. V.S. Barashenkov, F.G. Gereghi, A.S. Iljinov, G.G. Jonsson, V.D. Toneev, Nucl. Phys. A **231**, 462 (1974).
9. M. Blann, B.L. Berman, T.T. Komoto, Phys. Rev. C **28**, 2286 (1983).
10. H.H. Heckman, P.J. Lindstrom, Phys. Rev. Lett. **37**, 56 (1976).
11. D.L. Olson, B.L. Berman, D.E. Greiner, H.H. Heckman, P.J. Lindstrom, G.D. Westfall, H.J. Crawford, Phys. Rev. C **24**, 1529 (1981).
12. I.A. Pshenichnov, I.N. Mishustin, J.P. Bondorf, A.S. Botvina, A.S. Iljinov, Phys. Rev. C **57**, 1920 (1998).
13. I.A. Pshenichnov, I.N. Mishustin, J.P. Bondorf, A.S. Botvina, A.S. Iljinov, Phys. Rev. C **60**, 044901 (1999).
14. I.A. Pshenichnov, J.P. Bondorf, I.N. Mishustin, A. Ventura, S. Masetti, Phys. Rev. C **64**, 024903 (2001).
15. C. Scheidenberger, I.A. Pshenichnov, T. Aumann, S. Datz, K. Summerer, J.P. Bondorf, D. Boutin, H. Geissel, P. Grafstrom, H. Knudsen, H.F. Krause, B. Lommel, S.P. Moller, G. Munzenberg, R.H. Schuch, E. Uggerhoj, U. Uggerhoj, C.R. Vane, A. Ventura, Z.Z. Vilakazi, H. Weick, Phys. Rev. Lett. **88**, 042301 (2002).
16. N. Bohr, J.A. Wheeler, Phys. Rev. **56**, 426 (1939).
17. A. Bohr, *Proceedings of the International Conference on the Peaceful Uses of Atomic Energy, Geneva, 1955*, Vol. **2** (United Nations, New York, 1956) p. 151.
18. J.T. Caldwell, E.J. Dowdy, B.L. Berman, R.A. Alvarez, P. Meyer, Phys. Rev. C **21**, 1215 (1980).
19. J.T. Caldwell, E.J. Dowdy, R.A. Alvarez, B.L. Berman, P. Meyer, Nucl. Sci. Eng. **73**, 153 (1980).
20. B.L. Berman, J.T. Caldwell, E.J. Dowdy, S.S. Dietrich, P. Meyer, R.A. Alvarez, Phys. Rev. C **34**, 2201 (1986).
21. A. Leprêtre, R. Bergère, P. Bourgeois, P. Carlos, J. Fagot, J.L. Fallou, P. Garganne, A. Veyssière, R. Gobel, H. Ries, U. Kneissl, G. Mank, H. Ströher, W. Wilke, D. Ryckbosch, J. Jury, Nucl. Phys. A **472**, 533 (1987).
22. T. Frommhold, F. Steiper, W. Henkel, U. Kneissl, J. Ahrens, R. Beck, J. Peise, M. Schmitz, Phys. Lett. B **295**, 28 (1992).
23. T. Frommhold, F. Steiper, W. Henkel, U. Kneissl, J. Ahrens, R. Beck, J. Peise, M. Schmitz, I. Anthony, J.D. Kellie, S.J. Hall, G.J. Miller, Z. Phys. A **350**, 249 (1994).
24. N. Bianchi, E. De Sanctis, M. Mirazita, V. Muccifora, Phys. Rev. C **60**, 064617 (1999).
25. V. Muccifora, N. Bianchi, A. Deppman, E. De Sanctis, M. Mirazita, E. Polli, P. Rossi, R. Burgwinkel, J. Hannappel, F. Klein, D. Menze, W.J. Schwille, F. Wehnes, Phys. Rev. C **60**, 064616 (1999).
26. A.S. Iljinov, D.I. Ivanov, M.V. Mebel, V.G. Nedorezov, A.S. Sudov, G.Y. Kezerashvili, Nucl. Phys. A **539**, 263 (1992).
27. D.I. Ivanov, G.Y. Kezerashvili, A.I. L'vov, S.I. Mishnev, V.G. Nedorezov, I.Y. Protopopov, A.S. Sudov, Sov. J. Nucl. Phys. **55**, 1 (1992).
28. A.A. Kazakov, G.Ya. Kezerashvili, L.E. Lazareva, V.G. Nedorezov, A.N. Skrinsky, A.S. Sudov, G.M. Tumaikin, Yu.M. Shatunov, JETP Lett. **40**, 1271 (1984).
29. A.S. Iljinov, E.A. Cherepanov, S.E. Chigrinov, Sov. J. Nucl. Phys. **32**, 166 (1980), (Yad. Fiz. **32**, 322 (1980)).
30. A.S. Iljinov, M.V. Mebel, C. Guaraldo, V. Lucherini, E. De Sanctis, N. Bianchi, P. Levi Sandri, V. Muccifora, E. Polli, A.R. Reolon, P. Rossi, S. Lo Nigro, Phys. Rev. C **39**, 1420 (1989).
31. C. Guaraldo, V. Lucherini, E. De Sanctis, A.S. Iljinov, M.V. Mebel, S. Lo Nigro, Nuovo Cimento A **103**, 607 (1990).
32. J.D.T. Arruda-Neto, A. Deppman, N. Bianchi, E. De Sanctis, Phys. Rev. C **51**, 751 (1995).
33. P.P. Delsanto, A. Fubini, F. Murgia, P. Quarati, Z. Phys. A **342**, 291 (1992).
34. A. Deppman, O.A.P. Tavares, S.B. Duarte, E.C. de Oliveira, J.D.T. Arruda-Neto, S.R. de Pina, V.P. Likhachev, O. Rodriguez, J. Mesa, M. Goncalves, Phys. Rev. Lett. **87**, 182701 (2001).

35. A. Deppman, O.A.P. Tavares, S.B. Duarte, J.D.T. Arruda-Neto, M. Goncalves, V.P. Likhachev, E.C. de Oliveira, Phys. Rev. C **66**, 067601 (2002).
36. Ye.S. Golubeva, A.S. Iljinov, I.A. Pshenichnov, Phys. At. Nucl. **57**, 2007 (1994), (Yad. Fiz. **57**, 2084 (1994)).
37. A.S. Botvina, A.S. Iljinov, I.N. Mishustin, Nucl. Phys. A **507**, 649 (1990).
38. J.P. Bondorf, A.S. Botvina, A.S. Iljinov, I.N. Mishustin, K. Sneppen, Phys. Rep. **257**, 133 (1995).
39. K.K. Gudima, G.A. Ososkov, V.D. Toneev, Sov. J. Nucl. Phys., **21**, 138 (1975), (Yad. Fiz. **21**, 260 (1975)).
40. A. Leprêtre, H. Beil, R. Bergère, P. Carlos, J. Fagot, A. De Miniac, A. Veyssière, Nucl. Phys. A **390**, 221 (1982).
41. J.S. Levinger, Phys. Rev. **84**, 43 (1951).
42. A. Leprêtre, H. Beil, R. Bergère, P. Carlos, J. Fagot, A. De Miniac, A. Veyssière, Nucl. Phys. A **367**, 237 (1981).
43. J.M. Laget, Nucl. Phys. A **312**, 256 (1978).
44. B. Lott, F. Goldenbaum, A. Böhm, W. Bohne, T. von Egidy, P. Figuera, J. Galin, D. Hilscher, U. Jahnke, J. Jastrzebski, M. Morjean, G. Pausch, A. Péghaire, L. Pienkowski, D. Polster, S. Proschitzki, B. Quednau, H. Rossner, S. Schmid, W. Schmid, Phys. Rev. C **63**, 034616 (2001).
45. V. Weisskopf, Phys. Rev. **52**, 295 (1937).
46. G.D. Adeev, A.S. Botvina, A.S. Iljinov, M.V. Mebel, N.I. Pichasov, O.I. Serdyuk, INR Preprint-816/93, Moscow, 1993.
47. A.V. Ignatyuk, G.N. Smirenkin, A.S. Tishin, Sov. J. Nucl. Phys. **21**, 255 (1975), (Yad. Fiz. **21**, 485 (1975)).
48. A.V. Ignatyuk, K.K. Istekov, G.N. Smirenkin, Sov. J. Nucl. Phys. **29**, 450 (1979), (Yad. Fiz. **29**, 875 (1979)).
49. A.S. Iljinov, M.V. Mebel, N. Bianchi, E. De Sanctis, C. Guaraldo, V. Lucherini, V. Muccifora, E. Polli, A.R. Reolon, P. Rossi, Nucl. Phys. A **543**, 517 (1992).
50. W.D. Myers, W.J. Swiatecki, Ark. Fys. **36**, 343 (1967).
51. J.-J. Gaimard, K.H. Schmidt, Nucl. Phys. A **531**, 709 (1991).
52. J.B. Martins, E.L. Moreira, O.A.P. Tavares, J.L. Vieira, L. Casano, A. D'Angelo, C. Schaerf, M.L. Terranova, D. Babusci, B. Girolami, Phys. Rev. C **44**, 354 (1991).
53. W. Reisdorf, Z. Phys. A **300**, 227 (1981).
54. J. Töke, W.J. Swiatecki, Nucl. Phys. A **372**, 141 (1981).
55. J. Treiner, *IAEA Advisory Group Meeting on Basic and Applied Problems of Nuclear Level Densities, Upton, 1983*, Report BNL-NCS-51694, p. 383.
56. W.D. Myers, W.J. Swiatecki, Ann. Phys. (N.Y.) **84**, 186 (1974).
57. A. Heinz, K.-H. Schmidt, A.R. Junghans, P. Armbruster, J. Benlliure, C. Böckstiegel, H.-G. Clerc, A. Grewe, M. de Jong, J. Müller, M. Pfützner, S. Steinhäuser, B. Voss, Nucl. Phys. A **713**, 3 (2003).
58. W.J. Llope, P. Braun-Munzinger, Phys. Rev. C **41**, 2644 (1990).
59. B.L. Berman, S.C. Fultz, Rev. Mod. Phys. **47**, 713 (1975).
60. S.S. Dietrich, B.L. Berman, At. Data Nucl. Data Tables **38**, 199 (1988).
61. N. Bianchi, A. Deppman, E. De Sanctis, A. Fantoni, P. Levi Sandri, V. Lucherini, V. Muccifora, E. Polli, A.R. Reolon, P. Rossi, A.S. Iljinov, M.V. Mebel, J.D.T. Arruda-Neto, M. Anghinolfi, P. Corvisiero, G. Gervino, L. Mazzaschi, V. Mokeev, G. Ricco, M. Ripani, M. Sanzone, M. Taiuti, A. Zucchiatti, R. Bergère, P. Carlos, P. Garganne, A. Leprêtre, Phys. Rev. C **48**, 1785 (1993).
62. V. Lucherini, C. Guaraldo, E. De Sanctis, P. Levi Sandri, E. Polli, A.R. Reolon, A.S. Iljinov, S. Lo Nigro, S. Aiello, V. Bellini, V. Emma, C. Milone, G.S. Pappalardo, M.V. Mebel, Phys. Rev. C **39**, 911 (1989).
63. B.L. Berman, R.E. Pywell, S.S. Dietrich, M.N. Thompson, K.G. McNeill, J.W. Jury, Phys. Rev. C **36**, 1286 (1987).
64. T.A. Armstrong, W.R. Hogg, G.M. Lewis, A.W. Robertson, G.R. Brookes, A.S. Clough, J.H. Freeland, W. Galbraith, A.F. King, W.R. Rawlinson, N.R.S. Tait, J.C. Thompson, D.W.L. Tolfree, Phys. Rev. D **5**, 1640 (1972).
65. M. MacCormick, G. Audit, N. D'Hose, L. Ghedira, V. Isbert, S. Kerhoas, L.Y. Murphy, G. Tamas, P.A. Wallace, S. Altieri, A. Braghieri, P. Pedroni, T. Pinelli, J. Ahrens, R. Beck, J.R.M. Annand, R.A. Crawford, J.D. Kellie, I.J.D. MacGregor, B. Dolbilkin, A. Zabrodin, Phys. Rev. C **53**, 41 (1996); M. MacCormick, J. Habermann, J. Ahrens, G. Audit, R. Beck, A. Braghieri, G. Galler, N. D'Hose, V. Isbert, P. Pedroni, T. Pinelli, G. Tamas, S. Wartenberg, A. Zabrodin, Phys. Rev C **55**, 1033 (1997).
66. T.A. Armstrong, W.R. Hogg, G.M. Lewis, A.W. Robertson, G.R. Brookes, A.S. Clough, J.H. Freeland, W. Galbraith, A.F. King, W.R. Rawlinson, N.R.S. Tait, J.C. Thompson, D.W.L. Tolfree, Nucl. Phys. B **41**, 445 (1972).
67. R. Engel, J. Ranft, S. Roesler, Phys. Rev. D **55**, 6957 (1997).
68. W. Weise, Phys. Rep. **13**, 53 (1974).
69. G.R. Brookes, A.S. Clough, J.H. Freeland, W. Galbraith, A.F. King, T.A. Armstrong, W.R. Hogg, G.M. Lewis, A.W. Robertson, W.R. Rawlinson, N.R.S. Tait, J.C. Thompson, D.W.L. Tolfree, Phys. Rev. D **8**, 2826 (1973).
70. V.S. Barashenkov, F.G. Gereghi, A.S. Iljinov, V.D. Toneev, Nucl. Phys. A **222**, 204 (1974).
71. G.S. Sauer, H. Chandra, U. Mosel, Nucl. Phys. A **264**, 221 (1976).
72. A. Sierk, S. Mashnik, LANL Report LA-UR-98-5998 (1998).
73. S. Michalowski, D. Andrews, J. Eickmeyer, T. Gentile, N. Mistry, R. Talman, K. Ueno, Phys. Rev. Lett. **39**, 737 (1977).
74. P. Carlos, H. Beil, R. Bergère, B.L. Berman, A. Leprêtre, A. Veyssière, Nucl. Phys. A **378**, 317 (1982).
75. A. Veyssière, H. Beil, R. Bergère, P. Carlos, J. Fagot, A. Leprêtre, A. De Miniac, Z. Phys. A **306**, 139 (1982).
76. P. Carlos, H. Beil, R. Bergère, J. Fagot, A. Leprêtre, A. De Miniac, A. Veyssière, Nucl. Phys. A **431**, 573 (1984).
77. B.L. Berman, K.S. Dhuga, W.R. Dodge, B.G. Ritchie, Jefferson Lab Report, CLAS Note 92-010 (1992).